Parechovirus infections in human brain organoids: host immune response and not neuro-infectivity as a correlate of neuropathology

Pamela Capendale
Amsterdam UMC
Inés García-Rodríguez
Amsterdam UMC
Lance Mulder
Amsterdam UMC
Josse Depla
Amsterdam UMC
Eline Freeze
Amsterdam UMC
Gerrit Koen
Amsterdam UMC
Renata Vieira de Sá
Amsterdam UMC
Carlemi Calitz
Amsterdam UMC
Dasja Pajkrt
Amsterdam UMC, University of Amsterdam, Vrije Universiteit, Emma Children's Hospital
Adithya Sridhar
Amsterdam UMC https://orcid.org/0000-0003-2986-4884
Katja Wolthers
k.c.wolthers@amsterdamumc.nl

Academic Medical Center https://orcid.org/0000-0003-1617-7049

Article

Keywords: Parechovirus-A, echovirus, human cerebral organoids, unguided neural organoids, neurotropic model, interferon response

Posted Date: February 22nd, 2023

DOI: https://doi.org/10.21203/rs.3.rs-2556721/v1

Additional Declarations: Yes there is potential Competing Interest. JAD and RS are employees and/or shareholders of UniQure Biopharma B.V.

Version of Record: A version of this preprint was published at Nature Communications on March 21st, 2024. See the published version at https://doi.org/10.1038/s41467-024-46634-9.

Abstract

Parechovirus A (PeV-A) is a species in the *Picornaviridae* family that can cause a variety of diseases, mainly in children.The most prevalent genotype, PeV-A1, can causes mild respiratory and gastrointestinal symptoms while the second most prevalent genotype, PeV-A3 can elicit severe neurological disease such as meningoencephalitis in infants. The factors determining differential outcomes between genotypes are poorly understood. In this study, we investigated the viral dynamics and tropism of PeV-A1 and PeV-A3 infection in human induced pluripotent stem cell (hiPSC)-derived unguided neural organoids (UNOs). UNOs supported PeV-A1 and PeV-A3 replication, as measured by RT-qPCR and confirmed by TCID50. Both genotypes showed similar cell tropism and infected neurons and astrocytes. Despite replicating up to a higher titre as compared to PeV-A3, PeV-A1 infection showed no significant cytokine upregulation while PeV-A3 infection resulted in an increased production of IFN-λ1 and CXCL10. This effect was also seen for Echovirus 11, another picornaviruses resulting in neurological disease. Blocking the IFN-pathway with Ruxolitinib resulted in enhanced replication of PeV-A3 indicating IFN-mediated restriction of PeV-A3 replication. This genotype-specific immune response could explain the exacerbated PeV-A3 associated severe clinical neuropathology.

Introduction

Human parechoviruses, officially known as Parechovirus A (PeV-A), are common childhood pathogens in the *Picornaviridae* family with a potential for severe clinical manifestations in infants[1]. PeV-A has been shown to circulate in several countries such as the Netherlands[2], Japan[3], and the United States of America (USA)[4]. PeV-As are closely related to enteroviruses (EVs), showing similar clinical characteristics and outbreak potential. PeV-As are as prevalent as EVs and are the second leading cause of viral CNS infections in neonates[1]. The striking parallelism between PeV-A and EVs is highlighted by the initial classification of PeV-A as Echoviruses[5], a polyphyletic group of “orphan” viruses within the enterovirus genus that include neurotropic viruses such as Echovirus 11 (E11)[6-8].

The PeV-A species is subdivided into 19 genotypes with the most prevalent genotypes worldwide being PeV-A1 and PeV-A3[9]. Although both PeV-A1 and PeV-A3 can elicit gastrointestinal and respiratory disease, PeV-A3 is predominantly associated with central nervous system (CNS) disease[10,11]. Several PeV-A3 outbreaks have been reported globally, being the most recent one in the USA in 2022[12]. After infection of the primary replication sites (airway and/or intestinal epithelium) the virus can reach the blood stream causing sepsis-like illnesses and infect other organs[10], causing CNS-related diseases like transient paralysis[13], encephalitis[1,14], and meningitis[10,14]. Most of these cases occur in infants younger than three months with PeV-A3 detection in the cerebrospinal fluid (CSF)[10,15]. Short-term neurological sequelae have been reported in 5% of infected children increasing to nearly 27% on the long-term[16]. The most reported neurological sequelae are neurodevelopmental delays, impairment in auditory functions, or gross motor function delay[16,17]. Despite the remarkable differences in clinical presentation

between the genotypes and potential long-term consequences, the underlying reasons for the differences are yet to be discovered.

A possible explanation for this genotype-specific difference in disease could be related to a preference of PeV-A3 to infect CNS cell types as compared to PeV-A1. In this regard, we previously described that PeV-A3 strains show higher replication kinetics on a neural cell line (SH-SY-5Y) compared to PeV-A1 strains[18]. The main structural difference between both genotypes resides in their receptor-binding region. The VP1 of PeV-A1, but not of PeV-A3, contains an Arginyl-glycyl-Aspartic acid (RGD) motif, which enables PeV-A1 to bind to cell membrane bound integrins[19,20] suggesting differential receptor usage of PeV-A1 and -A3 for entry. This differential use could lead to a difference in cell tropism and disease presentation. Lastly, as PeV-A3 induced immune responses have been linked to the pathogenesis of PeV-A3[21,22], differences in genotype-specific immune responses is posed as an explanation for the differences in PeV-A1 and PeV-A3 induced clinical presentations.

Although immortalized cell lines and an animal model have been used to study PeV-A neuropathology[23], they come with several limitations. Models based on cell lines lack complexity and biological relevance[24], while animal models are often not susceptible to human viruses and do not recapitulate the human neurodevelopment[25,26]. Organoids address these shortcomings by not only closely recapitulating the cellular composition, structure, and complexity of the organ they mimic, but also the human neurodevelopment[24]. There are several types of organoids that mimic the brain with the two main subtypes being unguided neural organoids (UNOs)[27] and regionalized neural organoids. UNOs are 3-dimensional (3D) structures generated from human induced pluripotent stem cells (hiPSCs) that recapitulate characteristics of the developing human brain[28]. Compared to regionalized organoids UNOs encompass broader characteristics of the human CNS with different cell types and regions present as seen during human neurodevelopment[29]. UNOs mature in stages[52] and show genetic features[53] similar to the developing human embryonic brain.

UNOs and other brain organoid models have previously been used to study infection of various viruses[30]. For example, UNOs recapitulate Zika virus induced fetal microcephaly observed in patients[31,32]. Similarly, the use of UNOs has allowed for the study of herpes simplex virus 1 (HSV-1) reactivation[33], and when infected with human cytomegalovirus (HCMV), UNOs showed similar patterns to clinical brain specimens[34]. Multiple advantages of organoids over conventional models have been demonstrated for studying CNS-related viruses[30]. They have proven to be of great value to recapitulate cellular tropism and the effect of infection on the cellular organization[35-38]. These benefits show great promise for addressing the questions regarding the genotype-specific CNS pathology of PeV-A3.

In this study, we use UNOs to study the effects of viral infection with genotypes PeV-A1 and PeV-A3. Infection of UNOs with E11 are included as a neuropathogenic control that causes clinically similar neurological disease as described for PeV-A3[39]. Our aim is to identify the difference in neuropathological effects caused by neuropathogenic (par)echoviruses compared to the non-neuropathogenic PeV-A1

genotype and the mechanisms behind this by evaluating the viral replication kinetics, cell tropism, and immunological response.

Results

Unguided neural organoids resemble cytoarchitecture and spatial organisation of the developing human foetal brain

UNOs were cultured for 67 days (Figure 1A), to determine the cell types present their cytoarchitecture was assessed by immunofluorescence. At this UNO development stage, we expected the presence of progenitor zones surrounded by self-organized patterns of neurons and astrocytes[28]. Indeed, the generated UNOs featured typical ventricular-like zones (VZs) with neural progenitor cells ($SOX2^+$) in the centre. These VZs were surrounded by radially distributed mature neurons ($MAP2^+$) and specific astrocyte rich regions (GFAP+) (Figure 1B; Supplementary Movie 1). Moreover, the cortical regions within the UNOs displayed a stereotypical layered organization of the developing human brain as previously described[40,41]. These cortical regions included cells positive for neural progenitor cell marker $PAX6^+$ in the centre (VZ). We observed organized cell layers surrounding the VZ that expressed neural markers specific for early-born deep-layer neurons ($CTIP2^+$), and late-born superficial layer neurons ($SATB2^+$)[28,40] (Figure 1C). This indicates proper development and layer organization that is observed in the developing human fetal brain[41], hence presenting a good model for the study of viral CNS infection in neonates.

PeV-A1, PeV-A3, and E11 infect and replicate in UNOs

To compare infection dynamics of the two PeV-A genotypes, 67-day old UNOs were inoculated with PeV-A1, PeV-A3, and E11 (Figure 2A). We observed significant replication of E11 in UNOs with peak copy numbers on day three (Figure 2B). For both PeV-A1 and PeV-A3 infected UNOs a significant increase in viral RNA copies is shown over time (Figure 2B). However, the kinetics of PeV-A1 and PeV-A3 replication were different. PeV-A1 showed a similar replication to that of EV E11, while PeV-A3 showed a slower and lower replication compared to PeV-A1 and EV E11. The increase in RNA copies was related to active viral replication, as we observed a reduction in viral RNA copies over time when the viruses were heat-inactivated prior to inoculation (Supplementary Figure 1). Finally, to confirm the generation of infectious viral particles, a $TCID_{50}$ assay was performed. In accordance with the RT-qPCR data, there was a significant increase in $TCID_{50}$ over time for all three viruses, indicative of presence of infectious viral particles (Figure 2C).

No difference in cell tropism observed for PeV-A1, PeV-A3 and E11

Immunocytochemistry was used to visualize the viral tropism in UNOs and to identify possible changes in the organoid architecture often accompanying viral infection in different brain organoid models[42-44]. We did not observe any major changes in the cytoarchitecture of the UNOs as a result of the viral infection (Figure 3). UNOs infected with PeV-A1 (Figure 3B) or PeV-A3 (Figure 3C) showed positive dsRNA (indicative of viral infection) in astrocyte ($GFAP^+$) and neuron ($MAP2^+$) rich areas (Figure 4 and Supplementary Figure 3). Moreover, we did not observe dsRNA within VZs, suggesting that neural progenitor cells are likely not susceptible to PeV-A1 and A3 infection (Figure 3). Similarly, E11 was also mainly found in $GFAP^+$ and $MAP2^+$ areas (Supplementary Figure 2).

PeV-A3 and E11 induce an upregulation of immune responses in comparison to PeV-A1

We previously described that PeV-A3 infection of human airway epithelium upregulated the expression of several immune-related genes such as interferon (IFN) and NF-κB signaling[22]. Moreover, clinical data from PeV-A3 infected patients showed elevated levels of inflammatory cytokines e.g. IFN-α2, C-X-C motif chemokine ligand 10 (CXCL10), and monocyte chemoattractant protein 1 (MCP-1) in plasma[45]. To understand the effect of PeV-A infection on innate immune responses of UNOs, we analysed the expression of a panel of cytokines associated with PeV-A infection and key cytokines in the CNS inflammatory response[46]. PeV-A3 infected organoids showed a significantly higher expression of *CXCL10* and *IFN-B1* at 5dpi compared to PeV-A1 infected organoids (Figure 5A) that was maintained at 10 dpi (Figure 5B) although not significantly different.

Moreover, to further confirm the relation between PeV-A3 infection and the corresponding cytokine response, we measured the protein concentration of specific cytokines using a Luminex 10-plex assay. We found that several inflammatory cytokines such as IFN-λ1, IFN-β, and CXCL10 were significantly upregulated for PeV-A3 both at 5 dpi (Figure 5C) and 10 dpi (Figure 5D), while none of these cytokines were upregulated for PeV-A1 (Figure 5C-D). The upregulation pattern observed for PeV-A3 was similar to that of E11 (Figure 5C-D) suggesting an important role for the host immune response upon infection with these viruses that are associated with clinical CNS disease.

Blocking of the IFN-pathway enhances PeV-A3 replication

Since some of the highly upregulated cytokines, namely IFN-β, IFN-λ1, and CXCL10, are related to the IFN signalling, we further characterized the role of the IFN-pathway on PeV-A infection. This was done by blocking the Janus kinase-signal transduced and activator of transcription (JAK-STAT) pathway, that is activated upon IFN binding resulting in IFN-stimulated transcription genes (ISGs) [47]. This blocking was performed using the JAK1/2 inhibitor Ruxolitinib (Rux; INCB018424)[48]. Firstly, it was confirmed that Rux was able to block the JAK/STAT pathway in UNOs. Upon stimulation of organoids with 500 ng of IFN-β or IFN-λ3, Rux-treated UNOs showed downregulation of ISGs expression compared to non-treated controls

(Supplementary Figure 3). Next, we determined the effect of Rux treatment on viral ISGs induction and its effect on viral replication (Figure 6A-B). Rux treatment resulted in a downregulation of ISGs at 5 dpi specially for PeV-A3 (Figure 6C), that was maintained until 10 dpi (Supplementary Figure 4A).

At 5dpi, we observed the effect of Rux on PeV-A3 infected organoids that was reflected in an increase in viral RNA (Figure 6D) and infectious particles (Figure 6E). Although the effect of blocking the JAK-STAT pathway was clear at 10 dpi, we did not observe any significant increase in viral replication for any of the PeV-A strains at this time point (Supplementary Figure 4C-D). Together these results indicate that IFN plays a role in controlling PeV-A3 replication. No significant difference was found in either ISG expression or viral replication upon Rux treatment in E11 infected UNOs (Figure 6).

Discussion

Despite the importance of picornaviruses infections, such as PeV-A, for human health, the pathology caused by PeV-A genotypes is largely unknown, especially in the CNS where it can cause debilitating disease. In this paper, we expanded the current understanding of PeV-A infection pertaining to CNS disease in humans using human neural organoids. Our data indicates that genotype-specific differences are not due to neuroinfectivity as both PeV-A1 and PeV-A3 productively infected UNOs. Viral RNA co-localized within the same cell types following infection. The innate immune response of UNOs following PeV-A3 infection was significantly stronger than that of PeV-A1. PeV-A3 elicited strong inflammatory immune responses comparable to E11 infection, that is clinically characterised by a similar aggressive CNS disease as PeV-A3. Collectively our findings align with clinical observations and suggests a role for immune-mediated neuropathology in PeV-A3 infection.

Previous research from our laboratory showed that in a neuroblastoma cell line, PeV-A3 was more infectious compared to PeV-A1[18]. And studies in human-based *in vitro* models have shown that the cell tropism of PeV-A1 and PeV-A3 was similar in human airway epithelium but different in human intestinal epithelium[49,22]. We therefore hypothesized that the different CNS neuropathology between genotypes could be explained by a lack of neurotropism for PeV-A1 or a differential cell tropism.

In contrast to what was suggested in our previous data with cell lines, results from our study in UNOs showed no differences in cell tropism between the genotypes, with both genotypes infecting neurons and astrocytes. Moreover, we did not observe any viral infection in VZs that are mainly composed of neural progenitor cells. The cell types that were infected by PeV-A1 and PeV-A3 in UNOs were the same as for E11, and have also been shown to be infected in patients by other members of the *Picornaviridae* family causing similar neuropathology (meningitis, encephalitis, etc.), such as poliovirus[50] or EV-A71[51]. Interestingly, PeV-A1 has only been described to cause CNS symptoms in one outbreak in 1986[52] and has since then never been associated with CNS disease. Similar findings of clinically non-neurotropic viruses infecting human organoid models have been described previously for dengue virus[53,54]. It could be that the blood-brain barrier (BBB) shields the brain from certain potentially neurotropic viruses that are

therefore not able to reach the brain. This warrants further studies on the ability of different PeV-A genotypes to bypass the BBB and to initiate CNS infection.

The main difference between genotypes observed in this study was related to the elicited innate immune response. Notably, despite PeV-A1 replicating faster and to a higher titre in the UNOs as compared to PeV-A3 and EV E11, no upregulation of cytokines was observed upon infection. On the other hand, our positive control virus, E11, showed an enhanced production of several cytokines/chemokines including IFN-λ1, CXCL10 or MCP-1, that have also been associated with E11 infection in the clinic[55] and in an *in vivo* mouse model[56]. Similarly, PeV-A3 induced a significant upregulation of IFN-λ1 and IFN-β that has also been observed in humans[45]. In addition, CXCL10 which is upregulated upon IFN signaling[57], was also upregulated in our organoids which indicates an important role for the IFN pathway in controlling PeV-A3 infection. This role for the IFN signalling pathway was further confirmed by enhanced viral replication upon inhibition of the JAK/STAT pathway with Rux. For PeV-A1 and E11, we did not observe any significant increase in replication upon Rux treatment. This could indicate that activation of the JAK/STAT pathway may be weaker for PeV-A1 and E11 as compared to PeV-A3 or that other mechanisms are involved in controlling viral cerebral spread. In the case of PeV-A1, where we did not observed any increase in IFN production, it is possible that the virus circumvents triggering the IFN pathway, as described for many other viruses (Japanese Encephalitis virus, Rubella virus, Hendra virus, Dengue virus) that have developed ways to escape the host immune response[58]. Further studies accounting for the other innate immune pathways ought to be performed to confirm this possible explanation.

CXCL10 (or IP-10) is pivotal for attracting inflammatory leukocytes across the blood-brain barrier (BBB) and therefore, plays an important role during neuroinflammation. It can be expressed by both neurons and astrocytes and is highly upregulated in astrocytes following viral infections[59]. CXCL10 has previously been shown to play either a protective or detrimental role in neuropathology caused by viruses, such as lymphocytic choriomeningitis virus, West Nile virus, and Herpes Simplex Virus[57]. Interestingly, PeV-A3 infection is usually associated with leukopenia in both the plasma and CSF[60], which may indicate that patients are not able to respond to CXCL10 signaling. We did not observe any significant upregulation of MCP-1, a pivotal chemokine of the CNS that is upregulated in PeV-A3 infected patients[45]. This could be explained by the high levels of MCP-1 in mock-infected organoids likely due to hypoxia at the organoid core due to the lack of a vasculature[61],[62].

On a broad note, a strong immune response in the CNS is usually associated with meningitis, encephalitis, and meningoencephalitis[63], suggesting that more profound immune responses might explain the PeV-A3 associated clinical manifestations. This could also explain why this disease is usually associated with young neonates as their immature immune system may not yet be capable of controlling viral spread[64]. This hypothesis is supported by other findings *in vivo* and *in vitro*[23], suggesting an increased innate antiviral immune response as a possible explanation for the clinical manifestations of PeV-A3.

In conclusion, we showed that brain organoids are a useful model to study genotype-specific characteristics of PeV-A infection of the CNS. PeV-A1 and PeV-A3 were able to infect these organoids without any apparent differences in cell tropism. PeV-A3, most commonly associated with CNS disease in humans, showed an upregulated immune response and enhanced replication upon blocking of the JAK/STAT pathway. We hypothesize that this may be related to the pathogenesis of PeV-A3 and its preferential infection of neonates. This hypothesis is further supported by similar observations upon E11 infection of UNOs.

Limitations

Although more complex than 2D models based on cell lines, UNOs still lack the full cell composition of the human brain, as they do not contain some key cell types such as microglia. The contribution of immune cells in this model will be highly interesting as they are vital in viral neuropathology and the corresponding immune response to infection. Furthermore, as previously mentioned , our model lacks vasculature and the BBB (and other CNS barriers) which may be an important factor in the genotype specific neuropathology of PeV-A. For this study UNOs, rather than region specific neural organoids, were used to ensure that a broad range of CNS regions were represented in the model. The inconsistency in cell number and composition that are associated with UNOs[65] compromise reproducibility. Future studies could use organoids with a guided protocol that contain neurons and astrocytes and are more consistent in size and composition, such as dorsal forebrain organoids[66,67]. Moreover, the use of other CNS models such as the choroid-plexus organoids[68] would allow the study of PeV-A3 presence in CSF and the role of the CSF barrier in PeV-A infection.

Materials And Methods

Cell lines and virus strains

Human colorectal adenocarcinoma cells (HT-29, ATTC HTB-38), rhesus monkey kidney cells (LLCMK2, provided by the Municipal Health Services, the Netherlands), and African green monkey kidney cells (Vero, provided by the National Institute of Public Health and the Environment, RIVM, the Netherlands) were used for virus culture. All cell lines were maintained in Eagle's minimum essential medium (EMEM, Lonza) supplemented with 8% (v/v) heat-inactivated fetal bovine serum (FBS, Sigma-Aldrich), 100 U/mL penicillin/streptomycin (Pen-Strep, Lonza), 1% (v/v) non-essential amino acids (100x, ScienceCell Research Laboratories), and 0.1% (v/v) L-glutamine (Lonza). Cell lines were incubated at 37ºC, 5% CO_2 and 95% humidity and passaged every seven days using trypsin.

The PeV-A1 Harris strain was obtained from the RIVM and cultured on HT-29 cells. The PeV-A3 152037 strain, a Dutch isolate from 2001 adapted to cell culture, was cultured on LLCMK2 cells. The Echovirus 11 (E11) 50473 strain, a Dutch isolate from faecal material was cultured on Vero cells. Heat inactivated (HI)

controls were generated by incubating the virus stock in a water bath at 65ºC for 20 min and infection was performed as described previously.

Human induced pluripotent stem cell culture

Human induced pluripotent stem cells (hiPSCs) (IMR90-4, WiCell) were cultured on human laminin 521 (Biolamina) – coated culture treated six-well plates and maintained in mTeSR+ medium (STEMCELL Technologies) supplemented with 1% (v/v) Pen-Strep. Cells were maintained at 37°C with 5% CO_2, passaged weekly with ReLeSR™, and subcultured in mTeSR+ medium with 10 µM Y-27632 Rho Kinase (ROCK) inhibitor (Cayman Chemical Company). Lines were kept in culture with removal of differentiated patches when necessary and regular testing for mycoplasma was performed.

Generation of unguided neural organoids

UNOs were generated from the IMR90 hiPSC (WiCell®) using the Cerebral Organoid Generation and Maturation kit from STEMCELL™ Technologies, that is based on the protocol described for UNOs generation by Lancaster *et al*[28]. In short, hiPSCs were detached into a single cell suspension using Gentle Cell Dissociation Reagent (STEMCELL™ Technologies) and seeded in an ultra-low attachment round bottom 96 well-plate (Corning) with embryoid body (EB) Formation Medium to obtain EBs. Hereafter, induction of neuroectoderm was obtained using Induction Medium (STEMCELL™ Technologies) followed by expansion of neuroepithelia by embedding EBs in ESC-qualified Matrigel (Corning) and culturing in Expansion Medium (STEMCELL™ Technologies). On day ten the organoids were placed on an orbital shaker (66 rpm) in Maturation Medium (STEMCELL™ Technologies) and medium was refreshed every 3-4 days until infection at day 67.

Infection of unguided neural organoids

UNOs from three independent batches were infected in technical triplicates with 10^5 50% tissue culture infectious dose ($TCID_{50}$) per mL of the different viruses. Individual organoids were placed on a round bottom 96-well plate coated with Anti-Adherence Rinsing Solution (STEMCELL™ Technologies) and 100 µL of the virus inoculum were added. Organoids were incubated for 2 h at 37ºC with 5% CO_2, washed three times with phosphate buffer saline (PBS, Lonza), and moved to a freshly coated 48-well plate with 500 µL of Maturation Medium (STEMCELL™ Technologies). After 10 min incubation the 0 h time-point was collected, and medium was replenished. Collection with full medium replenishment was repeated at 1-, 3-, 5-, 7-, and 10-days post infection (dpi).

RT-qPCR

RNA was isolated from 25 µL of the collected supernatant using the Bioline Isolate II RNA mini kit (Meridian Bioscience®) following the manufacturer´s instructions. Equal volumes of the eluted RNA were used for reverse-transcription and 5 µL of the cDNA was used for reverse-transcription quantitative PCR (RT-qPCR). qPCR was performed on a CFX Connect Real-Time PCR Detection System (Bio-Rad), and C_q values were transformed into viral genome copies using a standard curve with known concentrations of the viral genomes. For RT-qPCR primers see Supplementary Table 1.

To analyse cytokine expression UNOs were harvested in RLY lysis buffer (Bioline Isolate II RNA mini kit (Meridian Bioscience®)) and stored at -80°C until RNA isolation. The sample was thoroughly homogenized by vortexing and resuspension by pipetting before RNA was isolated. The same protocol as described previous was used for RNA extraction, cDNA synthesis, and RT-qPCR. Cytokine upregulation was measured using primer sets (see Supplementary Table 1, Biolegio) where expression of the target gene was normalized to reference genes. The combination of RPLP0 and RPLP2 was chosen as most stably expressed set of reference genes under both mock and virus infected organoids using Normfinder[69]. Gene expression was normalized using the method[70] using the geometric mean of both reference genes. Infected samples were normalized to the uninfected control to visualize the effect of infection on cytokine expression in the UNOs.

$TCID_{50}$

Supernatant samples (25 µL) of multiple time-points were titrated for each virus, where PeV-A1 was titrated on HT-29, PeV-A3 was titrated on LLCMK2 and E11 was titrated on Vero cells. Briefly, ten-fold dilutions of each sample were performed and seeded in a 96-well plate (50 µL), the appropriate cells were added (200 µL) and incubated for 10 days until readout. For the readout, the cells were examined for the appearance of cytopathic effect and the $TCID_{50}$ was calculated using the Reed and Muench Method[71] and normalized to the 0 h time-point to determine the increase of infectious particles over time.

Immunofluorescence staining

Organoids were fixed at 5 and 10 dpi with 4% (v/v) formaldehyde (Sigma-Aldrich) in PBS for 30 min at room temperature (RT). After fixation organoids were washed three times with PBS and incubated in 30% (w/v) sucrose (Merck) by overnight incubation at 4°C. The organoids were embedded in optimal cutting temperature compound (OCT, Tissue Tek) snap frozen on dry ice, and stored at -80°C until sectioning. 20 µm sections were cut using a cryostat (NX71, Thermo Fisher Scientific) and collected on SuperFrost Plus slides (Thermo Scientific). Sections were stored at -80°C until staining. For immunostaining, sections were blocked for 2 h at RT in a blocking solution consisting of 10% (v/v) SeaBlock Blocking Buffer (Thermo Scientific) with 1% (v/v) Triton X-100 (Sigma) in PBS. After blocking, primary antibodies (Supplementary Table 2) were added in 1:1 blocking solution:PBS and incubated overnight at 4°C. Sections were washed three times with PBS for 5 min, and incubated with secondary antibody

(Supplementary Table 2) solution and Hoechst (Thermo Fisher Scientific) at RT for 1 h. Samples were quenched using ReadyProbes Tissue Autofluorescence Quenching kit (Invitrogen, kit) and incubated for 5 min, followed by 3 PBS washes. Finally, slides were mounted with glass coverslips using ProLong Gold Antifade Mounting Medium (Invitrogen). UNOs were imaged using Leica TCS SP8-X microscope and Leica LAS AF Software (Leica Microsystems). Z-stacks were also taken, and 3D reconstructions were made using the LAS-X 3D software (Leica Microsystems).

Ruxolitinib treatment

UNOs were pretreated with 5 μM or vehicle dimethyl sulfoxide (DMSO, Santa Cruz Biotechnology) and incubated for 1 h before infection at 37°C. After pre-treatment organoids were stimulated with 500 ng interferon (IFN) β (R&D Systems), or IFN-λ3 (R&D Systems), or infected as described previously with PeV-A1, PeV-A3, or E11. Treatment with 5 μM Rux/vehicle was continued throughout the 10 days post infection with every medium change at 1-, 3-, 5-, 7-, and 10dpi.

Procartaplex Multiplex Immunoassay

To detect cytokines, present in supernatant samples of (un)infected brain organoids, a customized 10-plex Luminex® assay was used (Procartaplex Multiplex Immunoassay, Invitrogen). Samples were lysed with 12.5% (v/v) Cell Lysis Buffer (Invitrogen) to inactivate viruses and the measurement was performed following the manufacturer's instructions. Fluorescence was measured using a Luminex (R&D) and from this cytokine concentrations were calculated using the provided standard curve in the kit. Values that were below the lower limit of detection (LLOD) were replaced by the LLOD/[72].

Statistical analysis

All statistical analysis was performed using GraphPad Prism 8 (GraphPad Software Inc.). experiments were performed in three independent organoid batches in triplicates (unless otherwise indicated). Data are presented as geometric mean ± geometric SD. The specific statistical tests performed for each analysis are indicated in the correspondent figure legend. Differences were considered significant when the *p*-value was <0.05.

Abbreviations

2D 2-Dimensional

3D 3-Dimensional

BBB Blood-brain barrier

CNS Central Nervous System

CSF Cerebrospinal Fluid

CXCL10 C-X-C motif chemokine ligand 10

DMSO Dimethyl sulfoxide

dpi Days post-infection

E11 Echovirus 11

EB Embryoid body

EMEM Eagle's minimum essential medium

FBS Fetal bovine serum

HCMV Human cytomegalovirus

HI Heat-inactivated

hiPSCs Human induced pluripotent stem cells

HSV-1 Herpes simplex virus 1

IFN Interferon

ISG Interferon-stimulated gene

JAK-STAT Janus kinase-signal transduced and activator of transcription

LLOD Lower limit of detection

MCP-1 Monocyte chemoattractant protein 1

OCT Optimal cutting temperature compound

PeV Parechovirus

PeV-A Parechovirus A

RGD Arginyl-glycyl-Aspartic acid

ROCK Rho Kinase

RT Room temperature

RT-qPCR Reverse-transcribed quantitative polymerase chain reaction

Rux Ruxolitinib

SD Standard deviation

$TCID_{50}$ 50% tissue culture infectious dose

UNOs Unguided neural organoids

USA United States of America

VZs Ventricular-like zones

ZIKV Zika virus

Declarations

Acknowledgements

All schematic representations were created with BioRender.com. Daisy Picavet from the core facility Cellular Imaging of the Amsterdam UMC (Amsterdam, the Netherlands) is acknowledged for her help with confocal imaging. We would also like to thank the Municipal Health Services and the National Institute of Public Health and the Environment (RIVM) for the supply of the cell lines.

Data availability statement

The raw data supporting the conclusions of this article is available in figshare.com and can be shared upon request.

Conflict of interest

JAD and RS are employees and/or shareholders of UniQure Biopharma B.V. The remaining authors declare that the research was conducted in the absence of any commercial or financial relationships that could be construed as a potential conflict of interest.

Author Contributions

Conceptualization: PC, IG-R, DP, AS, and KW. Data curation: PC, IG-R, LM, EF, JD, GK, and RV-S. Formal analysis: PC, IG-R. Funding acquisition: AS, DP, and KW. Investigation: PC, IG-R, LM, EF, JD, GK, and RV-S. Methodology: PC, IG-R, LM, EF, JD, GK, and RV-S. Project administration: AS, DP, and KW. Supervision: CC,

RV-S, AS, DP, and KW. Validation: PC, IG-R. Visualization: PC, IG-R. Writing of the original draft: PC, IG-R and AS. Writing, review and editing: PC, IG-R, LM, EF, JD, GK, CC, RS-V, AS, DP, and KW. As described by CRediT-Contributor Roles Taxonomy (casrai.org). All authors contributed to the article and approved the submitted version.

Funding

This research was funded by the European Union's Horizon 2020 Research and Innovation Programme under the Marie Sklowdowska-Curie Grant Agreement OrganoVIR (grant 812673) and GUTVIBRATIONS (grant 953201), the PPP Allowance (Focus-on-Virus) made available by Health Holland, Top Sector Life Sciences & Health, to the Amsterdam UMC, location Amsterdam Medical Center to stimulate public–private partnerships, and the Van Herk group through a donation to Amsterdam UMC, location Academic Medical Center.

References

1. Wolthers, K. C. *et al.* Human parechoviruses as an important viral cause of sepsislike illness and meningitis in young children. *Clin Infect Dis* **47**, 358-363, doi:10.1086/589752 (2008).
2. van der Sanden, S. *et al.* Prevalence of human parechovirus in the Netherlands in 2000 to 2007. *J Clin Microbiol* **46**, 2884-2889, doi:10.1128/JCM.00168-08 (2008).
3. Watanabe, K., Hirokawa, C. & Tazawa, T. Seropositivity and epidemiology of human parechovirus types 1, 3, and 6 in Japan. *Epidemiol Infect* **144**, 3451-3460, doi:10.1017/S0950268816001795 (2016).
4. Abedi, G. R. *et al.* Enterovirus and Human Parechovirus Surveillance - United States, 2009-2013. *MMWR Morb Mortal Wkly Rep* **64**, 940-943, doi:10.15585/mmwr.mm6434a3 (2015).
5. Coller, B. A. *et al.* Echovirus 22 is an atypical enterovirus. *J Virol* **64**, 2692-2701, doi:10.1128/jvi.64.6.2692-2701.1990 (1990).
6. Halfon, N. & Spector, S. A. Fatal Echovirus Type 11 Infections. *American Journal of Diseases of Children* **135**, 1017-1020, doi:10.1001/archpedi.1981.02130350021008 (1981).
7. Abdullahi, A. M., Sarmast, S. T. & Singh, R. Molecular Biology and Epidemiology of Neurotropic Viruses. *Cureus* **12**, e9674, doi:10.7759/cureus.9674 (2020).
8. Tebruegge, M. & Curtis, N. Enterovirus infections in neonates. *Seminars in Fetal and Neonatal Medicine* **14**, 222-227, doi:https://doi.org/10.1016/j.siny.2009.02.002 (2009).
9. Brouwer, L., Betrian, M. R. E., Pajkrt, D., Wolthers, K. C. & World-Wide Prevalence and Genotype Distribution of Parechovirus A. *Virol. Retrovirol. J.* **2**, 1-7 (2019).
10. Romero, J. R. & Selvarangan, R. The human Parechoviruses: an overview. *Adv Pediatr* **58**, 65-85, doi:10.1016/j.yapd.2011.03.008 (2011).

11. Benschop, K. S. M. *et al.* Human Parechovirus Infections in Dutch Children and the Association between Serotype and Disease Severity. *Clinical Infectious Diseases* **42**, 204-210, doi:10.1086/498905 (2006).
12. CDC. *HAN00469*, <https://emergency.cdc.gov/han/2022/han00469.asp> (2022).
13. Ito, M., Yamashita, T., Tsuzuki, H., Takeda, N. & Sakae, K. Isolation and identification of a novel human parechovirus. *J Gen Virol* **85**, 391-398, doi:10.1099/vir.0.19456-0 (2004).
14. Verboon-Maciolek, M. A. *et al.* Human parechovirus causes encephalitis with white matter injury in neonates. *Ann Neurol* **64**, 266-273, doi:10.1002/ana.21445 (2008).
15. Harvala, H., Wolthers, K. C. & Simmonds, P. Parechoviruses in children: understanding a new infection. *Curr Opin Infect Dis* **23**, 224-230, doi:10.1097/qco.0b013e32833890ca (2010).
16. van Hinsbergh, T. M. T., Elbers, R. G., Hans Ket, J. C. F., van Furth, A. M. & Obihara, C. C. Neurological and neurodevelopmental outcomes after human parechovirus CNS infection in neonates and young children: a systematic review and meta-analysis. *The Lancet Child & Adolescent Health* **4**, 592-605, doi:10.1016/s2352-4642(20)30181-4 (2020).
17. Britton, P. N. *et al.* Parechovirus Encephalitis and Neurodevelopmental Outcomes. *Pediatrics* **137**, e20152848, doi:10.1542/peds.2015-2848 (2016).
18. Westerhuis, B. M. *et al.* Specific cell tropism and neutralization of human parechovirus types 1 and 3: implications for pathogenesis and therapy development. *J Gen Virol* **93**, 2363-2370, doi:10.1099/vir.0.043323-0 (2012).
19. Merilahti, P., Karelehto, E. & Susi, P. Role of Heparan Sulfate in Cellular Infection of Integrin-Binding Coxsackievirus A9 and Human Parechovirus 1 Isolates. *PLOS ONE* **11**, e0147168, doi:10.1371/journal.pone.0147168 (2016).
20. Triantafilou, K., Triantafilou, M., Takada, Y. & Fernandez, N. Human Parechovirus 1 Utilizes Integrins αvβ3 and αvβ1 as Receptors. *Journal of Virology* **74**, 5856-5862, doi:doi:10.1128/JVI.74.13.5856-5862.2000 (2000).
21. Sridhar, A., Karelehto, E., Brouwer, L., Pajkrt, D. & Wolthers, K. C. Parechovirus A Pathogenesis and the Enigma of Genotype A-3. *Viruses* **11**, doi:10.3390/v11111062 (2019).
22. Karelehto, E. *et al.* Polarized Entry of Human Parechoviruses in the Airway Epithelium. *Front Cell Infect Microbiol* **8**, 294, doi:10.3389/fcimb.2018.00294 (2018).
23. Jan, M. W., Su, H. L., Chang, T. H. & Tsai, K. J. Characterization of Pathogenesis and Inflammatory Responses to Experimental Parechovirus Encephalitis. *Front Immunol* **12**, 753683, doi:10.3389/fimmu.2021.753683 (2021).
24. Sridhar, A. *et al.* A Perspective on Organoids for Virology Research. *Viruses* **12**, doi:10.3390/v12111341 (2020).
25. Ayyavoo, V. Modeling Human Viral Diseases: Trials and Triumphs. *Frontiers in Virology* **1**, doi:10.3389/fviro.2021.722297 (2021).

26. Moreni, G. *et al.* Bridging the gap between emerging models and humans by learning from polio animal studies: A systematic review. *Clinical and Translational Discovery* **2**, doi:10.1002/ctd2.42 (2022).
27. Pașca, S. P. *et al.* A nomenclature consensus for nervous system organoids and assembloids. *Nature* **609**, 907-910, doi:10.1038/s41586-022-05219-6 (2022).
28. Lancaster, M. A. *et al.* Cerebral organoids model human brain development and microcephaly. *Nature* **501**, 373-379, doi:10.1038/nature12517 (2013).
29. Pasca, S. P. The rise of three-dimensional human brain cultures. *Nature* **553**, 437-445, doi:10.1038/nature25032 (2018).
30. Depla, J. A. *et al.* Human Brain Organoids as Models for Central Nervous System Viral Infection. *Viruses* **14**, doi:10.3390/v14030634 (2022).
31. Dang, J. *et al.* Zika Virus Depletes Neural Progenitors in Human Cerebral Organoids through Activation of the Innate Immune Receptor TLR3. *Cell Stem Cell* **19**, 258-265, doi:10.1016/j.stem.2016.04.014 (2016).
32. Cugola, F. R. *et al.* The Brazilian Zika virus strain causes birth defects in experimental models. *Nature* **534**, 267-271, doi:10.1038/nature18296 (2016).
33. D'Aiuto, L. *et al.* Modeling Herpes Simplex Virus 1 Infections in Human Central Nervous System Neuronal Cells Using Two- and Three-Dimensional Cultures Derived from Induced Pluripotent Stem Cells. *J Virol* **93**, doi:10.1128/JVI.00111-19 (2019).
34. Brown, R. M. *et al.* Human Cytomegalovirus Compromises Development of Cerebral Organoids. *J Virol* **93**, doi:10.1128/jvi.00957-19 (2019).
35. Bullen, C. K. *et al.* Infectability of human BrainSphere neurons suggests neurotropism of SARS-CoV-2. *ALTEX* **37**, 665-671, doi:10.14573/altex.2006111 (2020).
36. Jacob, F. *et al.* Human Pluripotent Stem Cell-Derived Neural Cells and Brain Organoids Reveal SARS-CoV-2 Neurotropism Predominates in Choroid Plexus Epithelium. *Cell Stem Cell* **27**, 937-950 e939, doi:10.1016/j.stem.2020.09.016 (2020).
37. Vahey, G. M., Lindsey, N. P., Staples, J. E. & Hills, S. L. La Crosse Virus Disease in the United States, 2003-2019. *Am J Trop Med Hyg* **105**, 807-812, doi:10.4269/ajtmh.21-0294 (2021).
38. Sridhar, A. *et al.* Enterovirus D68 Infection in Human Primary Airway and Brain Organoids: No Additional Role for Heparan Sulfate Binding for Neurotropism. *Microbiol Spectr* **10**, e0169422, doi:10.1128/spectrum.01694-22 (2022).
39. Wildenbeest, J. G. *et al.* Pleconaril revisited: clinical course of chronic enteroviral meningoencephalitis after treatment correlates with in vitro susceptibility. *Antivir Ther* **17**, 459-466, doi:10.3851/IMP1936 (2012).
40. Renner, M. *et al.* Self-organized developmental patterning and differentiation in cerebral organoids. *EMBO J* **36**, 1316-1329, doi:10.15252/embj.201694700 (2017).

41. Lancaster, M. A. & Knoblich, J. A. Organogenesis in a dish: Modeling development and disease using organoid technologies. *Science* **345**, 1247125, doi:doi:10.1126/science.1247125 (2014).
42. Brown, R. M. *et al.* Human Cytomegalovirus Compromises Development of Cerebral Organoids. *Journal of Virology* **93**, e00957-00919, doi:doi:10.1128/JVI.00957-19 (2019).
43. Qian, X., Nguyen, H. N., Jacob, F., Song, H. & Ming, G. L. Using brain organoids to understand Zika virus-induced microcephaly. *Development* **144**, 952-957, doi:10.1242/dev.140707 (2017).
44. Krenn, V. *et al.* Organoid modeling of Zika and herpes simplex virus 1 infections reveals virus-specific responses leading to microcephaly. *Cell Stem Cell* **28**, 1362-1379 e1367, doi:10.1016/j.stem.2021.03.004 (2021).
45. Sasidharan, A., Hassan, W. M., Harrison, C. J., Hassan, F. & Selvarangan, R. Host Immune Response to Enterovirus and Parechovirus Systemic Infections in Children. *Open Forum Infect Dis* **7**, ofaa261, doi:10.1093/ofid/ofaa261 (2020).
46. Michalska, A., Blaszczyk, K., Wesoly, J. & Bluyssen, H. A. R. A Positive Feedback Amplifier Circuit That Regulates Interferon (IFN)-Stimulated Gene Expression and Controls Type I and Type II IFN Responses. *Front Immunol* **9**, 1135, doi:10.3389/fimmu.2018.01135 (2018).
47. Ezeonwumelu, I. J., Garcia-Vidal, E. & Ballana, E. JAK-STAT Pathway: A Novel Target to Tackle Viral Infections. *Viruses* **13**, doi:10.3390/v13122379 (2021).
48. Good, C. W., A.I.; Coyne, C.B. Type III interferon signaling restricts enterovirus 71 infection of goblet cells. *Sci Adv.* **6**, eaau4255, doi:10.1126/sciadv.aau4255 (2019).
49. García-Rodríguez, I. *et al.* Parechovirus A Infection of the Intestinal Epithelium: Differences Between Genotypes A1 and A3. *Front Cell Infect Microbiol* **11**, 740662, doi:10.3389/fcimb.2021.740662 (2021).
50. Racaniello, V. R. One hundred years of poliovirus pathogenesis. *Virology* **344**, 9-16, doi:https://doi.org/10.1016/j.virol.2005.09.015 (2006).
51. Wong, K. T. *et al.* The Distribution of Inflammation and Virus in Human Enterovirus 71 Encephalomyelitis Suggests Possible Viral Spread by Neural Pathways. *Journal of Neuropathology & Experimental Neurology* **67**, 162-169, doi:10.1097/nen.0b013e318163a990 (2008).
52. Figueroa, J. P., Ashley, D., King, D. & Hull, B. An outbreak of acute flaccid paralysis in Jamaica associated with echovirus type 22. *J Med Virol* **29**, 315-319, doi:10.1002/jmv.1890290418 (1989).
53. Yoon, K. J. *et al.* Zika-Virus-Encoded NS2A Disrupts Mammalian Cortical Neurogenesis by Degrading Adherens Junction Proteins. *Cell Stem Cell* **21**, 349-358 e346, doi:10.1016/j.stem.2017.07.014 (2017).
54. Li, Y. *et al.* Induction of Expansion and Folding in Human Cerebral Organoids. *Cell Stem Cell* **20**, 385-396 e383, doi:10.1016/j.stem.2016.11.017 (2017).
55. Chonmaitree, T. & Baron, S. Bacteria and Viruses Induce Production of Interferon in the Cerebrospinal Fluid of Children with Acute Meningitis: A Study of 57 Cases and Review. *Reviews of Infectious Diseases* **13**, 1061-1065, doi:10.1093/clinids/13.6.1061 (1991).

56. Wells, A. I. & Coyne, C. B. An In Vivo Model of Echovirus-Induced Meningitis Defines the Differential Roles of Type I and Type III Interferon Signaling in Central Nervous System Infection. *J Virol* **96**, e0033022, doi:10.1128/jvi.00330-22 (2022).
57. McKimmie, C. & Michlmayr, D. Role of CXCL10 in central nervous system inflammation. *International Journal of Interferon, Cytokine and Mediator Research*, doi:10.2147/ijicmr.S35953 (2014).
58. Devasthanam, A. S. Mechanisms underlying the inhibition of interferon signaling by viruses. *Virulence* **5**, 270-277, doi:10.4161/viru.27902 (2014).
59. Elemam, N. M., Talaat, I. M. & Maghazachi, A. A. CXCL10 Chemokine: A Critical Player in RNA and DNA Viral Infections. *Viruses* **14**, 2445 (2022).
60. Sharp, J. *et al.* Characteristics of young infants in whom human parechovirus, enterovirus or neither were detected in cerebrospinal fluid during sepsis evaluations. *The Pediatric infectious disease journal* **32**, 213-216, doi:10.1097/INF.0b013e318276b328 (2013).
61. Nzou, G. *et al.* Multicellular 3D Neurovascular Unit Model for Assessing Hypoxia and Neuroinflammation Induced Blood-Brain Barrier Dysfunction. *Sci Rep* **10**, 9766, doi:10.1038/s41598-020-66487-8 (2020).
62. Vértesy, Á. *et al.* Gruffi: an algorithm for computational removal of stressed cells from brain organoid transcriptomic datasets. *The EMBO Journal* **41**, e111118, doi:https://doi.org/10.15252/embj.2022111118 (2022).
63. Koyuncu, O. O., Hogue, I. B. & Enquist, L. W. Virus infections in the nervous system. *Cell Host Microbe* **13**, 379-393, doi:10.1016/j.chom.2013.03.010 (2013).
64. Basha, S., Surendran, N. & Pichichero, M. Immune responses in neonates. *Expert Rev Clin Immunol* **10**, 1171-1184, doi:10.1586/1744666X.2014.942288 (2014).
65. Andrews, M. G. & Kriegstein, A. R. Challenges of Organoid Research. *Annu Rev Neurosci* **45**, 23-39, doi:10.1146/annurev-neuro-111020-090812 (2022).
66. Pasca, A. M. *et al.* Functional cortical neurons and astrocytes from human pluripotent stem cells in 3D culture. *Nat Methods* **12**, 671-678, doi:10.1038/nmeth.3415 (2015).
67. Yoon, S. J. *et al.* Reliability of human cortical organoid generation. *Nat Methods* **16**, 75-78, doi:10.1038/s41592-018-0255-0 (2019).
68. Pellegrini, L. *et al.* SARS-CoV-2 Infects the Brain Choroid Plexus and Disrupts the Blood-CSF Barrier in Human Brain Organoids. *Cell Stem Cell* **27**, 951-961 e955, doi:10.1016/j.stem.2020.10.001 (2020).
69. Andersen, C. L., Jensen, J.L., Ørntoft, T.F. Normalization of real-time quantitative reverse transcription-PCR data: a model-based variance estimation approach to identify genes suited for normalization, applied to bladder and colon cancer data sets. *Cancer Res.* **1**, 5245-5250, doi:10.1158/0008-5472.CAN-04-0496 (2004).
70. Livak, K. J. & Schmittgen, T. D. Analysis of Relative Gene Expression Data Using Real-Time Quantitative PCR and the 2−ΔΔCT Method. *Methods* **25**, 402-408, doi:https://doi.org/10.1006/meth.2001.1262 (2001).

71. Reed, L. J. & Muench, H. A SIMPLE METHOD OF ESTIMATING FIFTY PER CENT ENDPOINTS12. *American Journal of Epidemiology* **27**, 493-497, doi:10.1093/oxfordjournals.aje.a118408 (1938).
72. Croghan, C. W., Egeghy, P.P. *Methods of Dealing with Values Below the Limit of Detection using SAS*, <http://analytics.ncsu.edu/sesug/2003/SD08-Croghan.pdf (> (2003).

Figures

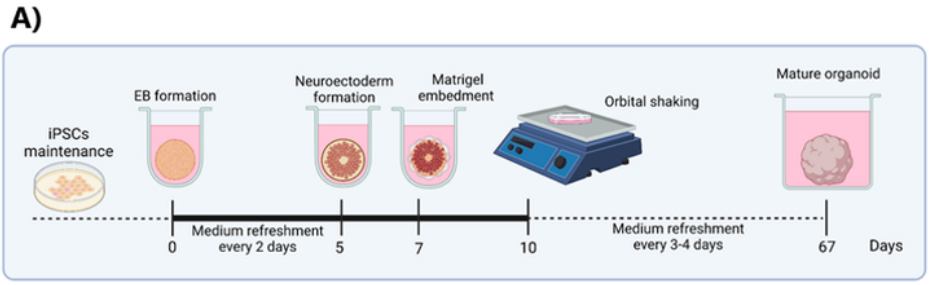

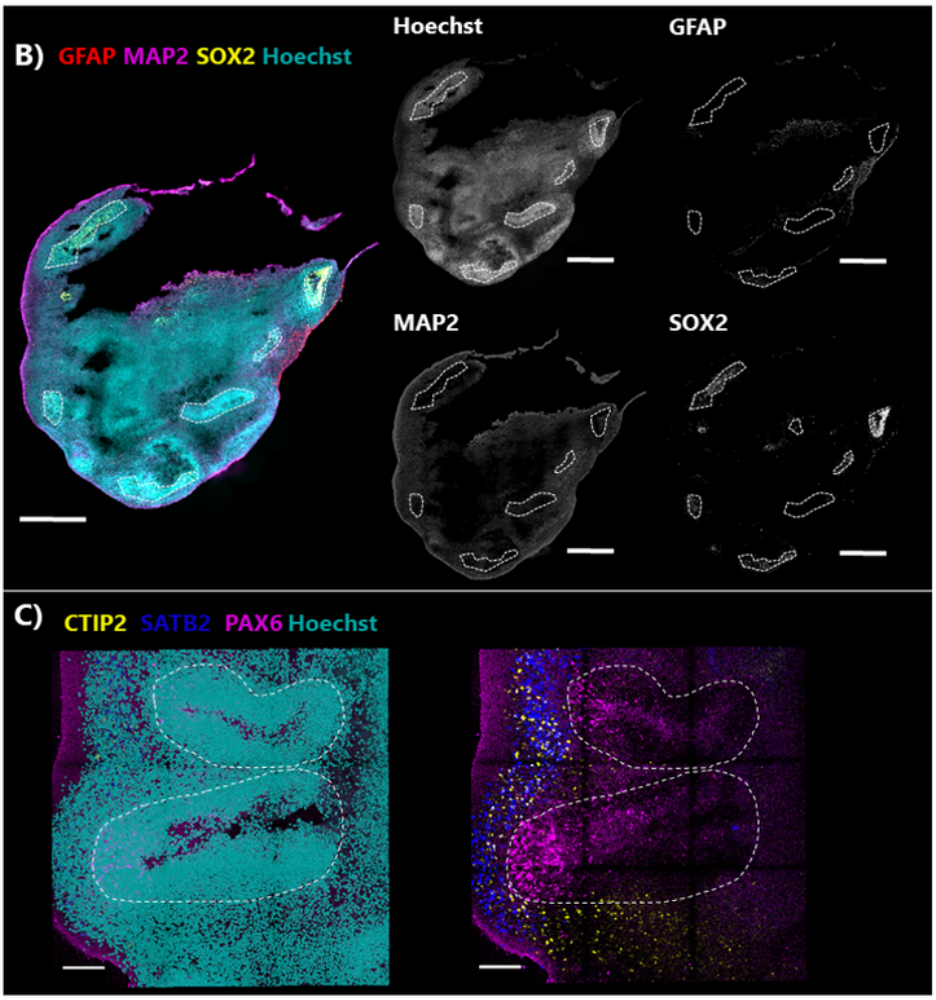

Figure 1

Characterization of unguided neural organoids by immunofluorescence staining. (A) Schematic representation of the protocol followed to obtain UNOs. **(B)** Representative image of an UNO section with the expected cytoarchitecture. Astrocyte-rich areas (GFAP, red) and neuron-rich areas (MAP2, magenta) are located outside the ventricular-like zones (VZs) that are high in neural progenitor cells (SOX2, yellow). Dashed lines are marked around VZs. Scale bar 500 µm. **(C)** Representative image of cortical neuron layering in UNOs. PAX6 staining (magenta) show neural progenitor cells in the VZs surrounded by early born deep-layer neurons (CTIP2, yellow), and late-born superficial layer neurons (SATB2, blue). Scale bar 100µm. In both cases nuclei were stained with Hoechst (cyan).

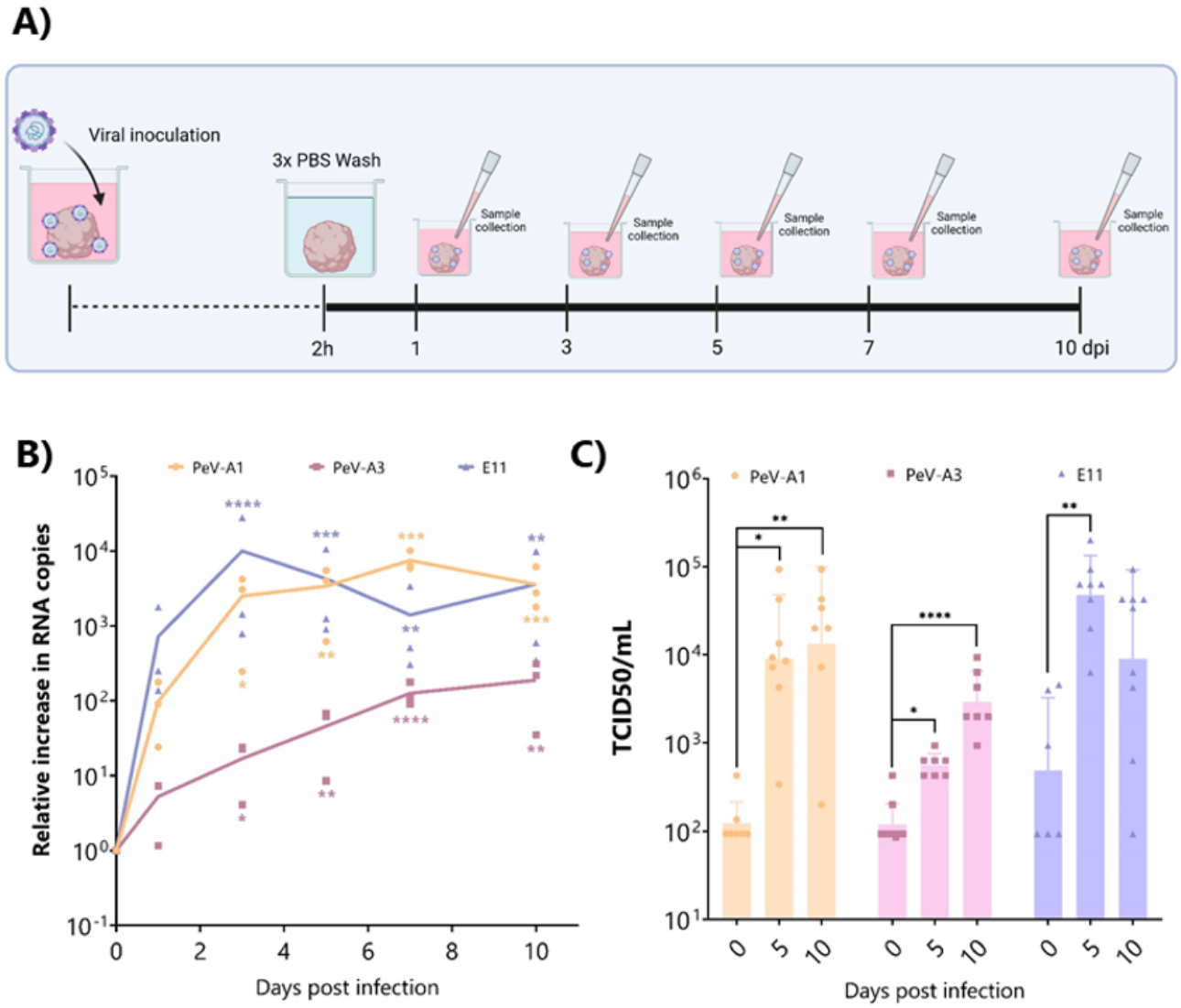

Figure 2

Replication kinetics of PeV-A1, PeV-A3, and E11 in unguided neural organoids. (A) Schematic representation and timeline of the infection of UNOs, (B) Relative increase in viral RNA copies in supernatant at different time points and, (C)Viral infectious particles from supernatant at 0, 5, and 10 dpi.

In all cases, data represents the geometric mean ± geometric standard deviation (SD) of three technical replicates for three batches of organoids (n=9). Statistical significance was analysed per virus using a Kruskal-Wallis test with multiple comparisons, * p-value < 0.05; ** p-value <0.01; *** p-value <0.001; **** p-value <0.0001.

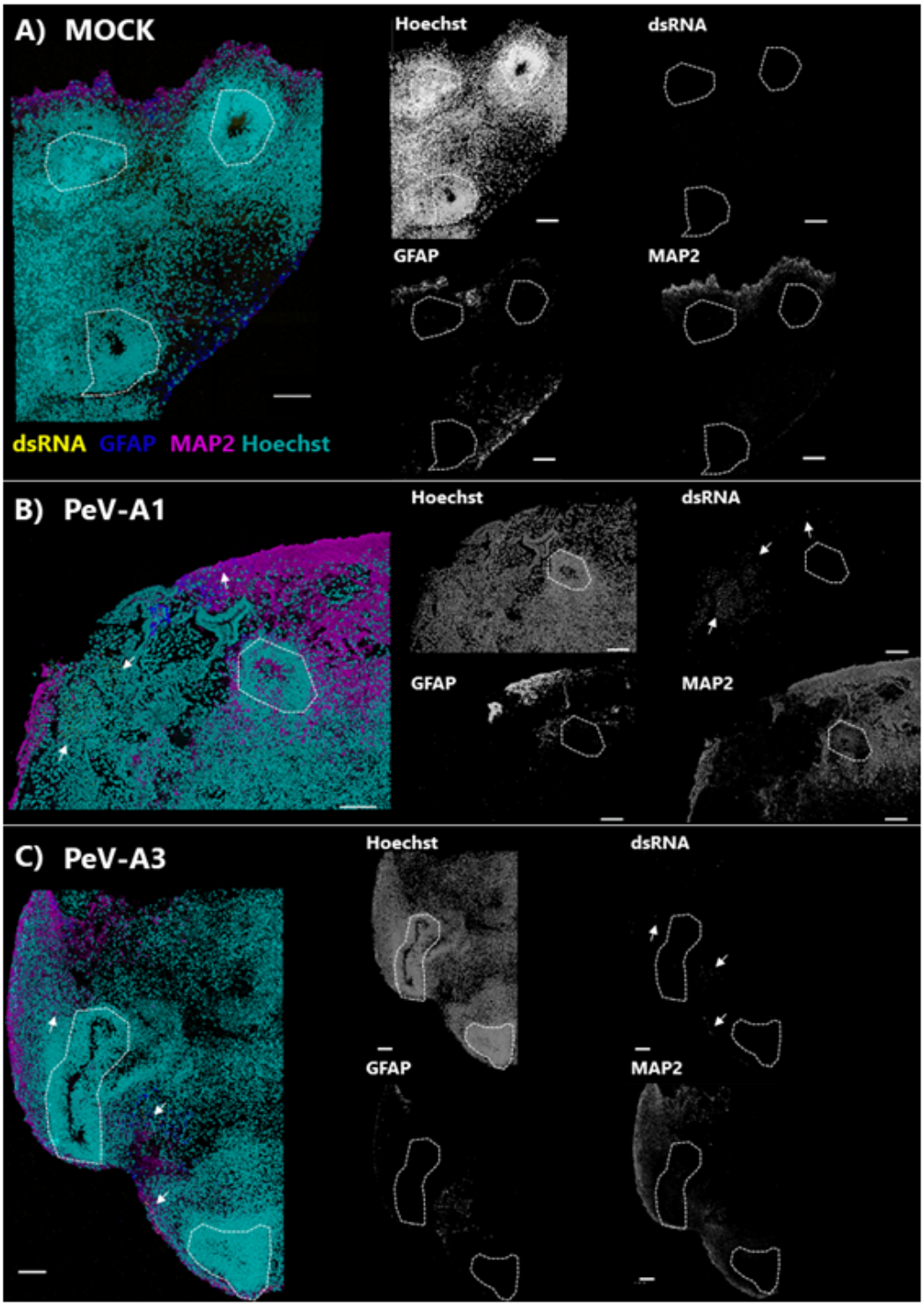

Figure 3

PeV-A1 and PeV-A3 localize outside ventricular-like zones (VZs). Representative confocal z-stacks from (A)MOCK, (B) PeV-A1, and (C) PeV-A3 infected UNOs at 10 dpi. Stained for nuclei (cyan), and immunolabelled for dsRNA (yellow), astrocytes (GFAP, blue) and neurons (MAP2,magenta). Dashed lines are around VZs. Scale bar 100 µm. Arrows indicate regions with positive dsRNA staining.

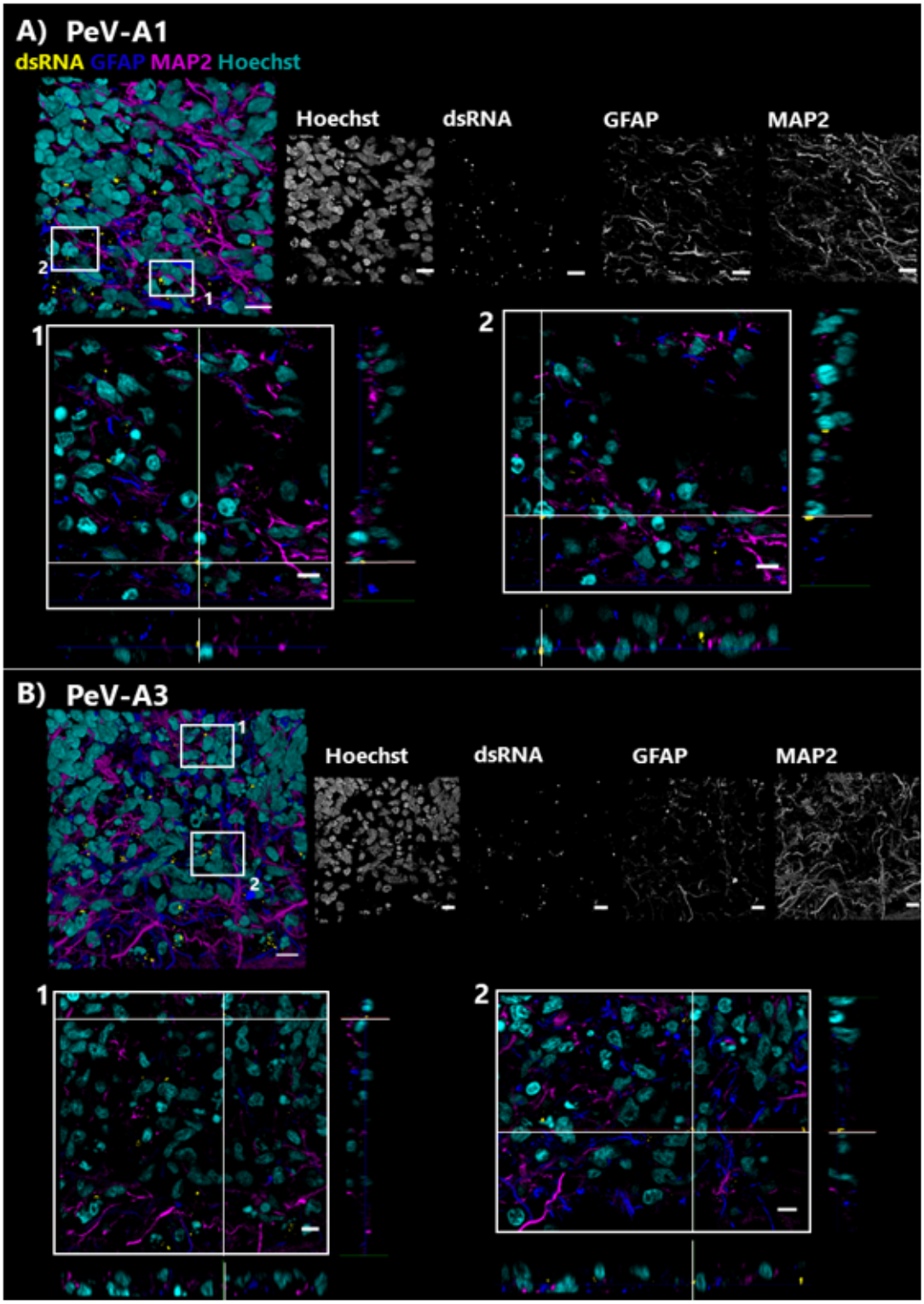

Figure 4

PeV-A1 and PeV-A3 co-localize with astrocyte and neuronal markers. Confocal z-stacks of (A)PeV-A1 and (B) PeV-A3 infected UNOs. Labelled for nuclei (cyan), and immunolabelled for dsRNA (yellow), astrocyte (GFAP, blue), and neurons (MAP2, magenta). Orthogonal view of areas in white boxes are shown below the 3D reconstructed z-stack. Scale bars 10 µm.

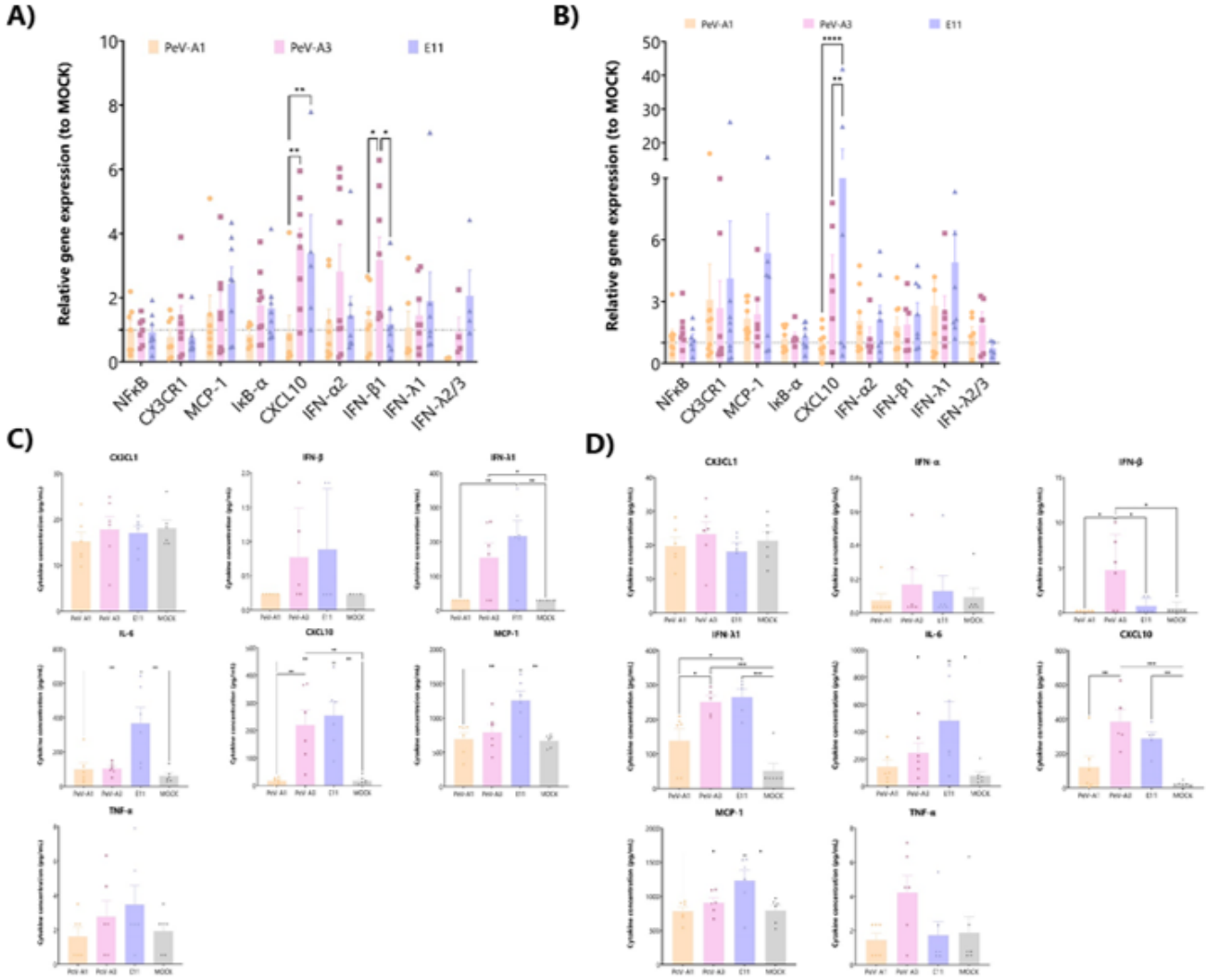

Figure 5

PeV-A3 leads to upregulation of the immune response. (A-B) Quantification of relative expression of cytokines to MOCK infected organoids at (A) 5dpi and (B)10 dpi by RT-qPCR. All data represents the geometric mean ± geometric SD of three technical replicates for three batches of organoids. Values above the dashed line represent an upregulation of the gene expression relative to the MOCK. Statistical significance was analysed by two-way ANOVA with Šídák's multiple comparisons tests for each specific cytokine. (C-D) Quantification of cytokines by Luminex present in supernatant of UNOs infected with PeV-A1, PeV-A3, E11, or MOCK infected at (C) 5dpi and (D) 10dpi. For (C)cytokines for which most values were below the LOD were removed. All data represents the geometric mean ± geometric SD of two technical replicates in three batches of organoids. Statistical significance was assessed using a One-way ANOVA

with Tukey's multiple comparisons for each cytokine individually, * p-value < 0.05; ** p-value <0.01; *** p-value <0.001; **** p-value <0.0001.

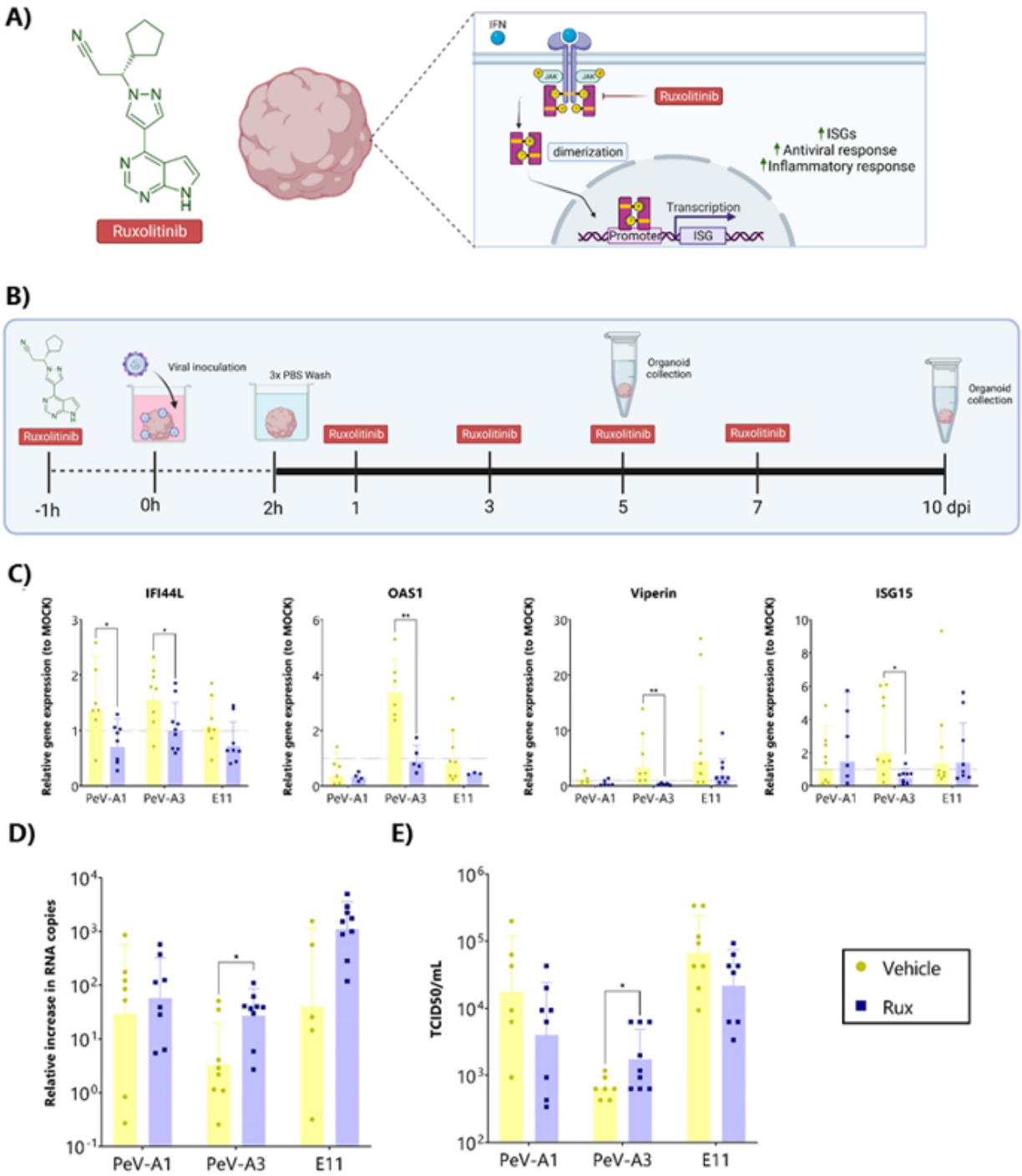

Figure 6

Ruxolitinib (Rux) treatment inhibits ISG activation and enhances PeV-A3 replication. (A) Schematic representation of the effect of Rux on the JAK/STAT pathway. (B) Timeline of Rux treatment on infected organoids. (C) ISGs gene expression at 5 dpi was normalized to reference genes and relative expression to MOCK infected organoids was calculated. (D) Relative increase in RNA copies at 5dpi for Rux or

DMSO-treated organoids from supernatant samples. (E) Virus titers at 5 dpi from supernatant collected samples of Rux or vehicle-treated organoids. Titers were determined by $TCID_{50}$. In all cases, data represents the geometric mean ± geometric SD of three technical replicates in three batches of organoids. Statistical significance was determined using a Student's t-test, * p-value < 0.05, ** p-value <0.01. For A-B values above the dashed line represent an upregulation of the gene expression relative to the MOCK.

Supplementary Files

This is a list of supplementary files associated with this preprint. Click to download.

- SupplementaryFiguremovieoverlayandchannels.mp4
- Supplementarymaterial.docx